# Subband–Landau-level coupling in GaAs/$Ga_{1-x}Al_xAs$ heterojunctions

A. D. Wieck,* F. Thiele, and U. Merkt
*Institut für Angewandte Physik, Universität Hamburg, Jungiusstrasse 11, D-2000 Hamburg 36, West Germany*

K. Ploog
*Max-Planck-Institut für Festkörperforschung, Heisenbergstrasse 1, Postfach 80 06 65, D-7000 Stuttgart 80, West Germany*

G. Weimann† and W. Schlapp
*Forschungsinstitut der Deutschen Bundespost, Postfach 5000, D-6100 Darmstadt, West Germany*
(Received 20 September 1988)

We study the coupling of Landau levels and electric subbands in quasi-two-dimensional electron inversion layers of modulation-doped GaAs/$Ga_{1-x}Al_xAs$ heterojunctions in tilted magnetic fields. We employ far-infrared Fourier-transform spectroscopy with light polarized parallel to the layers. When the subband separation $E_{10}$ is much larger than the cyclotron energy $\hbar\omega_c$, we find an enhancement of the cyclotron mass due to the parallel magnetic-field component. When the subband separation $E_{10}=r\hbar\omega_c$ is a multiple $r=1,2$ of the cyclotron energy, we observe a resonant splitting of the cyclotron resonance. The mass enhancement as well as the magnitudes and energetic positions of the splittings are described by perturbation theory and by the triangular-well approximation of the space-charge potential. From the experimental data we determine intersubband energies and dipole matrix elements. Both depend on electron density, which we adjust by illumination with a light-emitting diode or by a gate voltage applied between the inversion layer and a front gate.

## I. INTRODUCTION

In inversion layers of GaAs/$Ga_{1-x}Al_xAs$ heterojunctions the electrons are quantized into quasi-two-dimensional (2D) subbands. Complete quantization into highly degenerate Landau levels with a separate Landau ladder on top of each electric subband edge occurs in magnetic fields that are applied perpendicularly to the plane of free motion. In other words, electric subband and magnetic Landau quantization are uncoupled in perpendicular magnetic fields, and electric subband energies $E_i$ and Landau energies $\hbar\omega_c(n+\frac{1}{2})$ are additive.[1]

In magnetic fields with directions tilted away from the surface normal by a tilt angle $\theta$, coupling of the electric and magnetic quantization takes place.[2–5] As long as the spreads of the subband wave functions are small compared to the cyclotron radius ($L \ll l$), the resulting level structure is described to a rough approximation by the so-called $\cos\theta$ law.[6] This law states that there is a Landau ladder on top of each electric subband with level spacings $\hbar\omega_c\cos\theta$.

This simple picture of subband quantization in tilted magnetic fields breaks down when there is crossing of Landau levels belonging to different electric subbands. The most prominent example of such a situation is observed when the subband spacing $E_{10}=E_1-E_0$ equals the cyclotron energy $\hbar\omega_{c\perp}=e\hbar B_\perp/m^*$ of the perpendicular magnetic field component $B_\perp$.[7] Then, the Landau level $n=1$ of the ground subband crosses the Landau level $n=0$ of the first-excited subband, and splitting of cyclotron resonance into two branches occurs. The two resonances correspond to intersubband resonance and cyclotron resonance, respectively, and they exchange their characters at the crossing point.

This resonant subband–Landau-level coupling provides a simple and convenient method of determining subband spacings in GaAs/$Ga_{1-x}Al_xAs$ heterojunctions.[7–10] The experimental convenience arises because the light can be incident perpendicularly to the sample, and the accompanying light polarization parallel to the inversion layer excites intersubband resonance via cyclotron resonance. It is interesting to compare this configuration with experiments in a strip-line arrangement with perpendicular light polarization that directly couples to the intersubband resonance. In such a configuration, intersubband resonances $E_{10}$ with satellite peaks $E_{10}\pm r\hbar\omega_{c\perp}$ ($r=1,2,\ldots$) are observed in tilted magnetic fields.[11,12] The paramount observation of intersubband resonance is due to the perpendicular light polarization, but the occurrence of satellite peaks is as well a manifestation of the subband–Landau-level coupling as is the resonant splitting of cyclotron resonance.

In the present situation of light polarization parallel to the interface, we primarily observe cyclotron-resonance excitations. Both the excitations at resonant coupling ($\hbar\omega_{c\perp}\simeq E_{10}$) and cyclotron resonance in the nonresonant regime ($\hbar\omega_{c\perp}\ll E_{10}$) allow us to determine intersubband or dipole matrix elements. Results of perturbation theory that relate these matrix elements to observable splittings and cyclotron masses are described in Sec. II, together with exact results for the triangular-well approximation of the surface electric potential. In Sec. III we give a brief description of our samples and experimental setup. In Sec. IV A we present the experimental spectra and in Sec. IV B the resulting intersubband energies and matrix

 

elements. We conclude with a discussion and summary in Sec. V.

## II. THEORETICAL CONSIDERATIONS

### A. Perturbation theory

Electrons subjected to a space-charge potential $V(z)$ and a magnetic field $B$ whose direction is tilted with respect to the $z$ direction by the tilt angle $\theta$ are described by the Hamiltonian

$$H=-\frac{\hbar^2}{2m^*}\frac{\partial^2}{\partial x^2}+\frac{e^2B_\perp^2}{2m^*}x^2-\frac{\hbar^2}{2m^*}\frac{\partial^2}{\partial z^2}+V(z)$$
$$+\frac{e^2B_\parallel^2}{2m^*}z^2-\frac{e^2B_\parallel B_\perp}{m^*}xz \qquad (1)$$

in the effective-mass approximation with an isotropic effective mass $m^*$. To arrive at Eq. (1), we have chosen the gauge $(0, x\cos\theta - z\sin\theta, 0)B$ for the vector potential and have applied the transformation $x \rightarrow x-\hbar k_y/eB_\perp$ of the original $x$ coordinate. By this transformation, the Hamiltonian becomes independent of momentum $\hbar k_y$ and the common periodic boundary condition for the $x$ direction yields the degeneracy $eB_\perp/h$ of eigenenergies in tilted magnetic fields. This degeneracy is independent of the form of the potential $V(z)$ and is solely determined by the perpendicular component $B_\perp$.[13,14] The $x$- and $z$-dependent terms in the first line of Eq. (1) describe quantization into Landau levels $\hbar\omega_{c\perp}(n+\frac{1}{2})$ due to the perpendicular magnetic field component, and into electric subbands $E_i$ due to the space-charge potential, respectively. The $z^2$ term causes a positive diamagnetic shift due to the parallel component $B_\parallel$.[1] The last term in Eq. (1) is proportional to the product $xz$ and couples Landau and subband quantization at all angles $0<\theta<90°$.[15] Here, we focus on the consequences and the experimental possibilities that are offered by this coupling Hamiltonian to characterize the surface potential $V(z)$ and its wave functions in GaAs/$Ga_{1-x}Al_xAs$ heterojunctions.

The Hamiltonian in Eq. (1) is treated by common perturbation theory using the tilt angle $\theta$ as perturbational parameter ($\hbar\omega_{c\parallel}=\hbar\omega_{c\perp}\tan\theta \ll E_{10}$). We start from the unperturbed Hamiltonian for a purely perpendicular magnetic field ($\theta=0$), i.e., we choose products of Landau oscillator functions $|n\rangle$ and subband wave functions $|i\rangle$ as a basis.[16] We first discuss the degenerate situations $E_{i'i}=E_{i'}-E_i=r\hbar\omega_c$ ($r=1,2$) of level crossings and then treat the nonresonant regime $\hbar\omega_{c\perp}\ll E_{i'i}$.

In first-order perturbation theory,[7] there is no correction to the eigenenergies of zeroth order, $E_i+\hbar\omega_{c\perp}(n+\frac{1}{2})$, except for the degenerate situation $E_{i'}-E_i=\hbar\omega_{c\perp}$. This situation is commonly addressed as full-field coupling ($r=1$) and is depicted for subbands $i=0,1,2$ in Fig. 1(b). First-order perturbation theory for degenerate levels $|i,n\rangle$ and $|i',n-1\rangle$ yields the level splitting

$$\Delta E_{r=1}=\sqrt{2n}\,\tan\theta\left|\frac{z_{i'i}}{l_\perp}\right|E_{i'i}\ , \qquad (2)$$

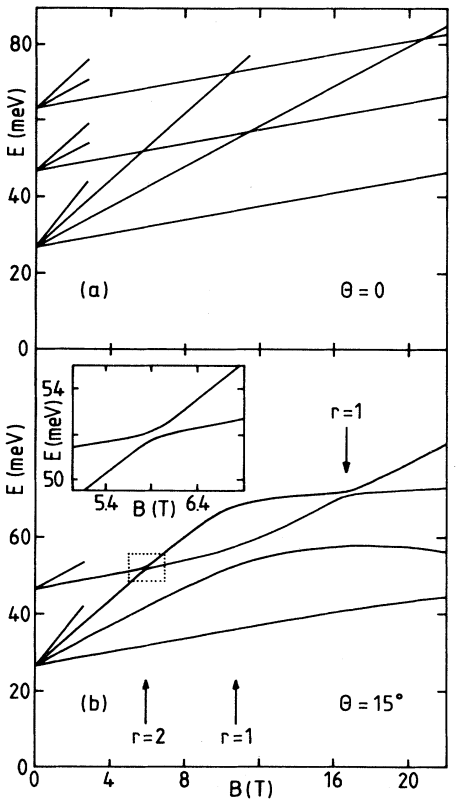


FIG. 1. Landau levels vs amplitude of magnetic field $B$ calculated in the triangular-well approximation ($m^*=0.066m_e$, $F_s=1.6\times10^4$ V cm$^{-1}$). (a) Perpendicular magnetic fields. (b) Tilted magnetic fields with anticrossing due to subband–Landau-level coupling. Full-field couplings ($r=1$) are evident at $B\simeq11$ and $\simeq17$ T when the spacings $E_{10}$ and $E_{20}$ of electric ($B=0$) subbands are approximately equal to the cyclotron energy $\hbar\omega_{c\perp}$ of the perpendicular field component $B_\perp$. The inset shows an enlarged view of the half-field coupling ($r=2$, $E_{10}\simeq2\hbar\omega_{c\perp}$) regime.

which is proportional to the intersubband or dipole matrix element $(z)_{i'i}=|\langle i'|z|i\rangle|$ normalized with the magnetic length $l_\perp=(\hbar/eB_\perp)^{1/2}$. As a consequence of the selection rule for the matrix elements $\langle n|x|n'\rangle=(n/2)^{1/2}l_\perp$ of the harmonic oscillator ($n'=n-1$), the degeneracy at a multiple $r$ is only removed by perturbation theory of order $r$. Hence, the splittings are proportional to the power $\tan^r(\theta)$ at small angles.

Important for experiments is the half-field coupling ($r=2$) because lower magnetic field strengths suffice.[9,10] There, the degeneracy is removed in second order and, consequently, the splitting is proportional to $\theta^2$ for small angles. As seen in Fig. 1(b) for the angle $\theta=15°$, the splitting is much smaller than the one at full-field coupling and, therefore, larger tilt angles must be employed in the experiments. The theoretical description of the splitting $\Delta E_{r=2}$ requires knowledge of diagonal and nondiagonal subband matrix elements $z_{i'i}$ and $(z^2)_{i'i}$, principally for all subbands $i$. Hence, it is particularly sensitive to the form

of the surface potential and its wave functions.

At all multiples $r$, both the diamagnetic and the coupling term of the Hamiltonian in Eq. (1) shift the energetic position of the gap center away from the position of the unperturbed crossings ($\theta=0$). Also the minimum gap energy does not exactly occur at the magnetic field $B_\perp = m^* E_{10}/re\hbar$, where the crossing in purely perpendicular magnetic fields takes place. This is clearly evident in Fig. 1(b) for full-field coupling ($r=1$) of subbands $E_0$ and $E_2$ at $B=17.7$ T.

Second-order effects also are apparent in the nonresonant regimes ($\hbar\omega_{c\perp} \ll E_{i'i}$) away from the level crossings. Perturbation theory of second order for nondegenerate levels gives the eigenenergies

$$E_{i,n} = E_i + \hbar\omega_{c\perp}(n+\tfrac{1}{2}) + \frac{e^2B_\parallel^2}{2m^*}[(z^2)_{ii} - (z_{ii})^2] - \frac{e^2B_\parallel^2}{2m^*}\sum_{i'(\neq i)} (z_{i'i})^2 \frac{1-\dfrac{E_{i'i}}{\hbar\omega_{c\perp}}(2n+1)}{1-\left[\dfrac{E_{i'i}}{\hbar\omega_{c\perp}}\right]^2} . \quad (3)$$

The first two terms represent the $\cos\theta$ law, the third one the diamagnetic shift, and the last one results from the coupling Hamiltonian.

In the nonresonant regimes, we observe cyclotron resonance previously[17] studied for the regime $\hbar\omega_{c\perp} \lesssim E_{10}/2$. The observed deviations of the cyclotron energy from the $\cos\theta$ law can be attributed to an angle-dependent mass $m_i^*(\theta)$ which is readily derived from Eq. (3):

$$\frac{m^*}{m_i^*(\theta)} = 1 - \tan^2\theta \sum_{i'(\neq i)} \frac{m^*(z_{i'i})^2 E_{i'i}}{\hbar^2} \frac{\left[\dfrac{\hbar\omega_{c\perp}}{E_{i'i}}\right]^2}{1-\left[\dfrac{\hbar\omega_{c\perp}}{E_{i'i}}\right]^2} . \quad (4)$$

Unlike the resonant splitting $\Delta E_{r=1}$ at full-field coupling described by Eq. (2), all matrix elements $z_{i'i}$ contribute to the apparent effective mass $m_i^*(\theta)$ in the nonresonant case. However, for cyclotron resonance in the ground electric subband $i=0$, the contribution of matrix elements $z_{i'0}$ ($i' \geq 2$) can be neglected to a good approximation.[17]

### B. Triangular-well approximation

The triangular-well approximation[1] of the potential $V(z)$ assumes that the electrons are confined by an infinitely high potential barrier at the $Ga_{1-x}Al_xAs$/GaAs interface ($z=0$), and by a potential $eF_sz$ with constant electric field $F_s$ inside the semiconductor GaAs. This model provides only a qualitative description, since it is not self-consistent, but it has the great advantage of the fact that all matrix elements can be given analytically. It also does not account for depolarization, i.e., the dynamical screening of the intersubband resonance (see Refs. 18–20), which will be discussed in Sec. V.

In the absence of a parallel magnetic field, the wave function of the electric subband $E_i$ is a normalized section of the Airy function

$$|i\rangle = N_i^{-1/2}\mathrm{Ai}(z/L - E_i/eF_sL) \quad (5)$$

with normalization constant $N_i = \mathrm{Ai}'(t_i)$. Here, the prime denotes the derivative with respect to the $z$ coordinate taken at the zero $t_i \simeq -[3\pi(i+\frac{3}{4})/2]^{2/3}$ of the Airy function. The $z$ coordinate is made dimensionless with the electric length $L = (\hbar^2/2m^*eF_s)^{1/3}$, and the subband edges

$$E_i \simeq \left[\frac{9\pi^2}{8m^*}\right]^{1/3} (e\hbar F_s)^{2/3}(i+\tfrac{3}{4})^{2/3} \quad (6)$$

follow from the boundary condition $\mathrm{Ai}(-E_i/eF_sL)=0$ at the interface.[1]

Calculation of precise eigenvalues in tilted magnetic fields requires numerical diagonalization of the full Hamilton matrix of Eq. (1). All matrix elements are readily calculated using analytical results[21] for integrals of the Airy function:

$$(z)_{i'i} = \begin{cases} -\frac{2}{3}t_iL, & i=i' \quad (7a) \\ \dfrac{2L}{(t_{i'}-t_i)^2}, & i\neq i' \quad (7b) \end{cases}$$

$$(z^2)_{i'i} = \begin{cases} \frac{8}{15}t_i^2L^2, & i=i' \quad (7c) \\ \dfrac{12L^2}{(t_{i'}-t_i)^4}, & i\neq i' . \quad (7d) \end{cases}$$

However, large matrices must be diagonalized to obtain convergent eigenenergies. To give an example, 50 Landau levels for each of five electric subbands are needed at a tilt angle $\theta \simeq 40°$.

The only fit parameter in the triangular-well model is the strength of the surface electric field $F_s$, which we choose to yield the desired subband spacing $E_{10}$. For a spacing $E_{10}=20$ meV, eigenenergies are depicted in Figs. 1(a) and 1(b) for tilt angles $\theta=0°$ and 15°. The dependence of the splittings $\Delta E_r$ on angle $\theta$ at full-field ($r=1$) and half-field coupling ($r=2$), as well as corresponding energies of gap centers $\bar{E}$, are shown in Figs. 2(a) and 2(b). At small angles, the splittings $\Delta E_{r=1}$ and $\Delta E_{r=2}$ increase linearly and quadratically with the tilt angle since they are first- and second-order effects, respectively. On the other hand, both shifts of the gap centers are second-order effects. It is interesting to note that at half-field coupling ($r=2$) the diamagnetic term in Eq. (3) dominates, causing a positive shift. At full-field coupling ($r=1$) the coupling term dominates, yielding a negative shift.

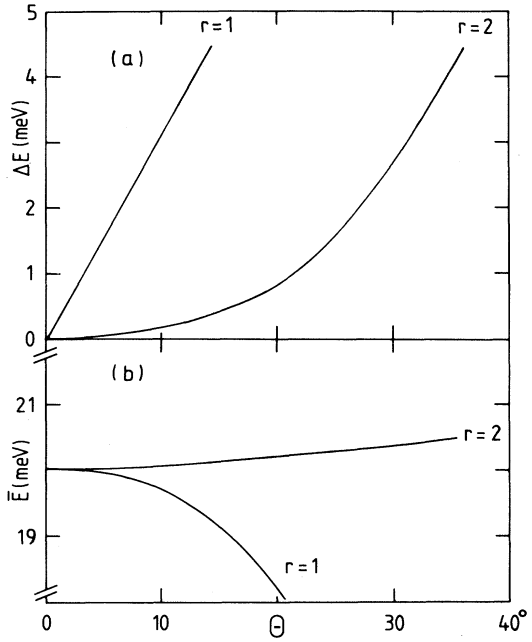


FIG. 2. (a) Gap energies $\Delta E$ and (b) gap centers $\bar{E}$ for full-field ($r=1$) and half-field ($r=2$) coupling of subbands $i=0,1$ vs tilt angle $\theta$. Gaps are determined by the minimum energy separation between split levels at a given angle. Parameters are the same as in Fig. 1.

## III. EXPERIMENTAL DETAILS

Samples are grown on semi-insulating GaAs substrates by molecular-beam epitaxy (MBE) using the modulation-doping technique.[22–24] To avoid Fabry-Pérot interferences in the spectroscopic experiments, the substrates are wedged by an angle of about 3°. Ohmic contacts to the inversion layers are prepared by diffusing Sn pellets at 400 °C for 5 min in a $N_2/H_2$ (95:5, in vol %) atmosphere. These contacts are connected to the electronic setup via In-soldered copper wires of diameter $\simeq 100$ $\mu$m. van der Pauw and Shubnikov–de Haas measurements reveal electron densities $N_s$ and dc mobilities $\mu$ which coincide within 10% with values determined from oscillator strengths and linewidths of the saturated cyclotron resonance in perpendicular magnetic fields.[25]

The carrier density is changed by illumination with band-gap radiation of a light-emitting diode (LED) prior to the experiment (LED) utilizing the persistent photoeffect or by a gate voltage $V_g$ applied between the inversion layers and semitransparent 5-nm-thick Ni-Cr front gates, which are evaporated onto the cap layers. Leakage currents $I \lesssim 1$ $\mu$A at voltages $V_g \simeq -1$ V cause only negligible pinch-off effects, i.e., inhomogeneities of the carrier density $N_s$ over the gate area of $\simeq 3\times 3$ mm$^2$. The experiments are carried out at liquid-helium temperatures $T \simeq 2$ K. We use a superconducting 12-T magnet or a resistive 20-T Bitter solenoid.

For reference purposes, in most experiments the inversion layer is first oriented perpendicularly to the magnetic field ($\theta=0°$) before it is tilted out of this position over a range of $\theta \leq 45°$ by means of a calibrated parallelogram mechanism which is incorporated into the sample holder. The transmitted far-infrared radiation is detected by a silicon bolometer which is placed inside the sample holder $\simeq 20$ cm away from the magnet center to eliminate the influence of the field on its sensitivity. The spectroscopic experiments are carried out in a fast-scan Fourier spectrometer (Bruker 113) using standard techniques.[26]

Transmittance spectra $T(B)$ are taken at constant magnetic fields $B$ and are normalized to the transmittance $T(B=0)$ in order to eliminate the frequency characteristic of the setup. To increase the signal-to-noise ratio further, gated samples are investigated in the following way. The magnetic field is kept constant. Then, at a particular gate voltage $V_g$, i.e., electron density $N_s$, the transmission is recorded in a sample file, and at the threshold voltage $V_{\rm th}$, i.e., density $N_s=0$, in a reference file, respectively. Switching between values $V_g$ and $V_{\rm th}$, typically each 30 s, and synchronously addressing the sample and the reference file, the spectra are co-added over typically 10 min. This leads to a very good suppression of eventual instrumental drifts and renders possible signal-to-noise ratios $\simeq 0.1\%$ in the normalized spectra $T(V_g)/T(V_{\rm th})$.

## IV. EXPERIMENTAL RESULTS

### A. Spectra

Fourier-transform spectra near full-field coupling are depicted in Fig. 3 for a sample of relatively high electron density $N_s = 6.0\times 10^{11}$ cm$^{-2}$ generated by LED illumination. The spectra are taken subsequently in the dark at

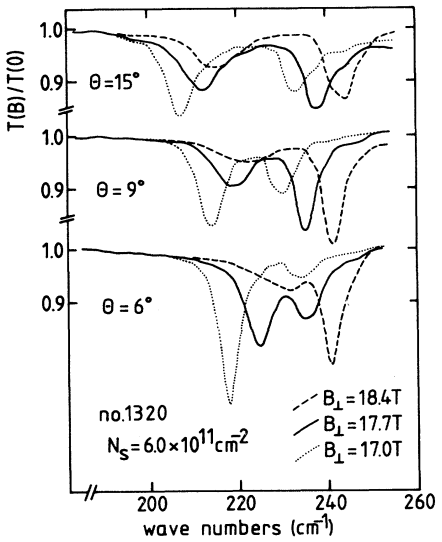


FIG. 3. Fourier-transform spectra for three tilt angles $\theta$ and magnetic field components $B_\perp$. Ratios of transmittances $T(B)/T(B=0)$ are plotted near full-field coupling ($E_{10} \simeq \hbar\omega_{c\perp}$).

three values of the perpendicular magnetic field component $B_\perp$ for each of three tilt angles $\theta$. At the lowest angle $\theta=6°$, the oscillator strengths of the split resonances are comparable at $B_\perp=17.7$ T (solid line). At a slightly lower component $B_\perp=17.0$ T (dotted line), the stronger resonance at 219 $cm^{-1}$ is cyclotron-like and the weaker one at 235 $cm^{-1}$ is intersubband-like. This situation is reversed at a higher component $B_\perp=18.4$ T (dashed line). Principally, this exchange of oscillator strength is observed at all tilt angles. However, the asymmetry of the oscillator strength becomes less at higher angles, which we interpret as being due to stronger coupling of cyclotron and intersubband resonance. Also as a result of enhanced coupling, the splitting of the resonances increases from $\theta=6$ to 15° and the gap center shifts to lower wave numbers by $\simeq 6$ $cm^{-1}$. The splittings and shifts will be analyzed further in the next section.

Spectra near full-field coupling of a sample with a low electron density $N_s=0.9\times10^{11}$ $cm^{-2}$ are shown in Fig. 4. The spectra of this ungated sample are taken without preceding LED illumination. Already at the angle $\theta=0.5°$, clear splitting is observed, and a wide gap is opened at $\theta=5.5°$, indicating particularly strong coupling of subbands $i=0$ and 1 in this sample. The spectra obviously demonstrate the formation of the gap by reduced oscillator strengths near the coupling regime. In fact, one can draw envelope functions to the dips whose minima yield the gap positions. The resonance positions are summarized in Fig. 5. As a further consequence of increased coupling at higher tilt angles, the positions of the

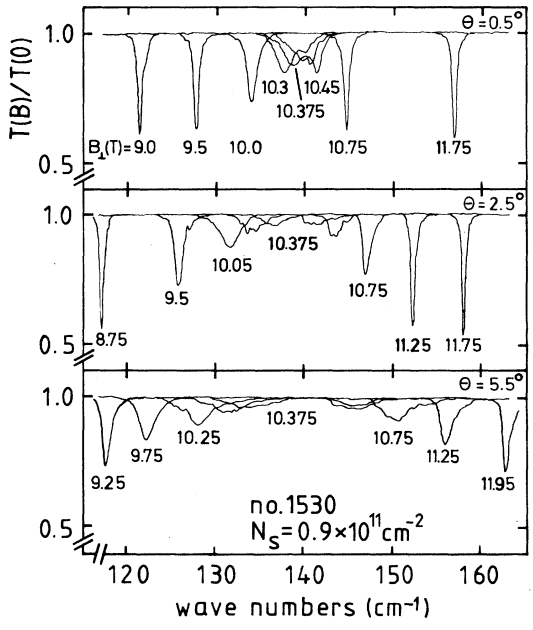


FIG. 4. Fourier-transform spectra near full-field coupling for three tilt angles $\theta$. Numbers near transmittance minima indicate magnetic field components $B_\perp$. The gap positions ($\simeq 140$ $cm^{-1}$) illustrate themselves by reduced oscillator strengths in their vicinity.

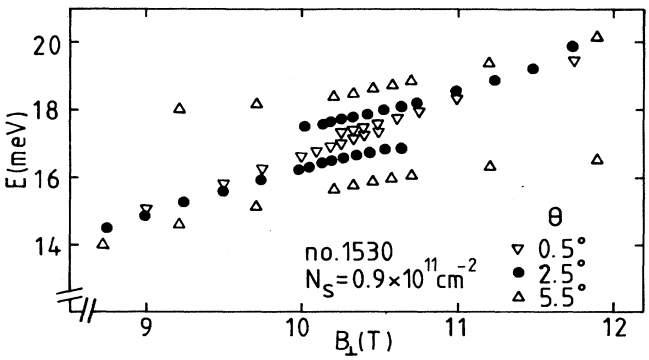


FIG. 5. Resonance positions for the spectra of Fig. 4. At the highest tilt angle $\theta=5.5°$, split cyclotron resonances can be detected in a comparatively wide range of magnetic fields.

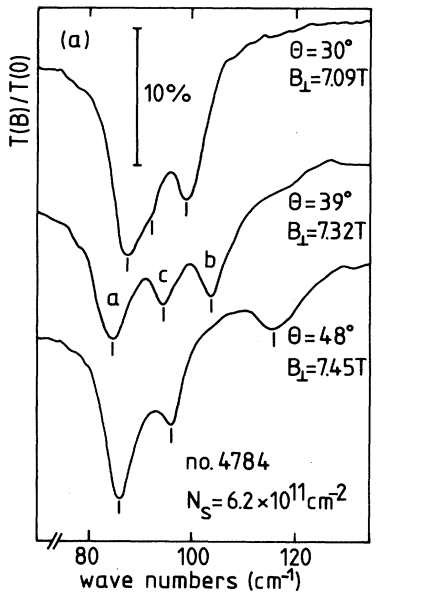


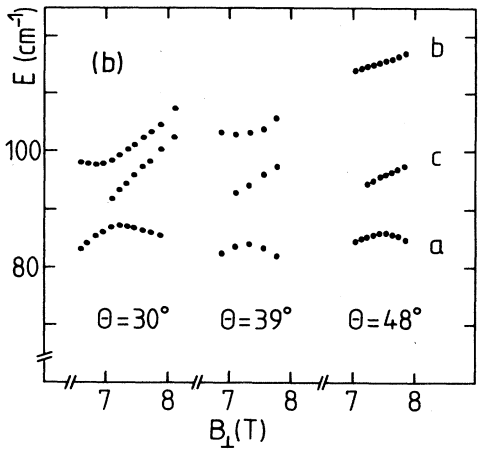


FIG. 6. (a) Spectra near half-field coupling ($E_{10}\simeq 2\hbar\omega_{c1}$). Resonances $a$ and $b$ are due to the splitting of cyclotron resonance $n=1\rightarrow2$ in the ground electric subband. Resonance $c$ represents $n=0\rightarrow1$ transitions. (b) Resonance positions.

intersubband-like resonances can be detected in a wider range of magnetic fields. In this sample, the center of the gap shifts by only $\simeq 2$ cm$^{-1}$ to lower wave numbers in the range $\theta = 0.5° - 5.5°$.

Spectra near half-field coupling for a sample with a high electron density $N_s = 6.2 \times 10^{11}$ cm$^{-2}$, which again is obtained by LED illumination, are depicted in Fig. 6(a). Here we observe three resonances labeled *a*, *b*, and *c*. Resonances *a* and *b* represent split cyclotron resonances between Landau levels $n = 1$ and 2. Note that rather large angles ($\theta = 30° - 48°$) are required to observe significant splittings. The splitting increases with tilt angle, but unlike full-field coupling the center of the gap between resonances *a* and *b* shifts to higher wave numbers as the tilt angle is increased. This is most clearly seen in Fig. 6(b), where the resonance positions are shown. For angles $\theta = 30°$ and 39°, the positions of resonances *a* and *b* exhibit a maximum and a minimum, respectively. This is characteristic for half-field coupling, since it is not observed at full-field coupling.

Resonance *c* is due to cyclotron transitions between Landau levels $n = 0$ and 1, which contribute to the spectra since their final state $n = 1$ is only partly occupied. To give an example, we have the filling factor $\nu = 3.5$ at the magnetic field $B_\perp = 7.32$ T. It is also interesting to note that the slope of the data points of resonance *c* in Fig. 6(b) is decreased significantly at the angle $\theta = 48°$, compared to the situation at smaller tilt angles. This is a consequence of nonresonant mass enhancement described by Eq. (4), since cyclotron resonance *c* is only affected by nonresonant subband–Landau-level coupling at magnetic fields $B_\perp \simeq 7.5$ T. Resonant coupling for the underlying $0 \rightarrow 1$ transitions becomes effective as full-field coupling only at higher magnetic fields $B_\perp \simeq 15$ T.

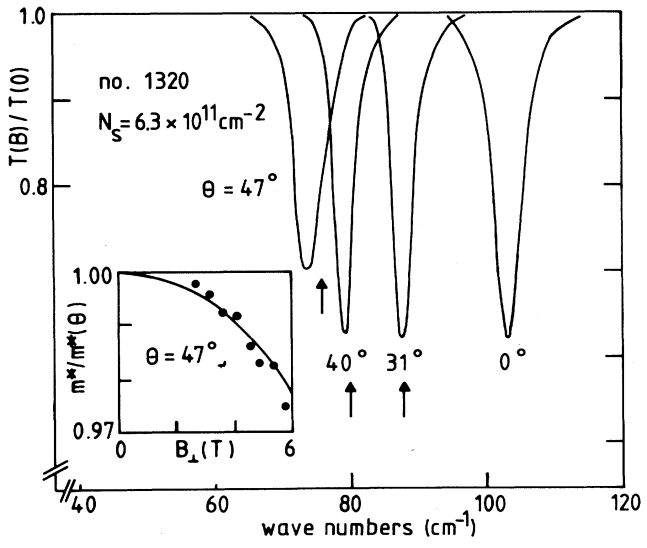


FIG. 7. Cyclotron resonances in the nonresonant regime ($\hbar\omega_{c\perp} \lesssim E_{10}/2$) for $B = 7.8$ T. Resonance frequencies obtained from the $\theta = 0°$ resonance assuming the $\cos\theta$ law are indicated by arrows. The inset shows the mass ratio $m^*(\theta = 0°)/m^*(\theta)$ vs component $B_\perp$. The solid line is calculated from Eq. (4) for $n = 1$ and matrix element $z_{10} = 22$ Å.

Cyclotron resonances in the nonresonant regime $\hbar\omega_{c\perp} \lesssim E_{10}/2$ are depicted in Fig. 7 for angles $\theta = 0° - 47°$. The arrows mark resonance positions that are expected when the $\cos\theta$ law is applied to the position of the resonance in the perpendicular magnetic field ($\theta = 0°$). For angles $\theta = 40°$ and 47°, the experimental positions lie clearly below the values predicted by the $\cos\theta$ law. This is described in Eq. (4) by the angle-dependent mass $m^*(\theta) = eB_\perp/2\pi c\bar{\nu}$ defined with the resonance wave number $\bar{\nu}$. In accordance with Eq. (4), the ratio $m^*/m^*(\theta)$ of masses $m^*$ and $m^*(\theta)$, measured in perpendicular ($\theta = 0°$) and tilted fields ($\theta = 47°$), is plotted in the inset of Fig. 7. This way of presenting the data is not only very sensitive, but also largely compensates for the dependence of the cyclotron mass on the filling factor $\nu = hN_s/eB_\perp$. This dependence has been attributed to band nonparabolicity,[27,28] polarons,[29,30] and many-body effects.[28,31–33]

The solid line in the inset is calculated from Eq. (4) with the matrix element $z_{10} = 22$ Å, which yields the best description of the experimental points. The influence of subbands $i' \geq 2$ is neglected, since the contribution of higher subbands to the mass enhancement is estimated[17] to be less than 10%.

### B. Subband energies and matrix elements

Intersubband energies $E_{10}$ can be evaluated from spectra recorded near the regime of full-field coupling ($r = 1$) as well as from traces taken near half-field coupling ($r = 2$). In both cases, the center of the energy gap between two split cyclotron resonances must be determined.[10] As soon as the value $E_{10}$ is known, the splitting $\Delta E_{r=1}$ gives the matrix element $z_{10}$, according to Eq. (2). This is true as long as the depolarization shift is small.[8] This, in fact, is the case in our heterojunctions, as will be discussed in Sec. V.

Most precise values of the gap centers, i.e., intersubband energies, are obtained if the positions of the split resonances are plotted versus magnetic field component $B_\perp$ at a fixed angle $\theta$. This we have done in Figs. 5 and 6(b) for full-field and half-field coupling, respectively. In the case of full-field coupling ($r = 1$), the gap center is taken at the magnetic field component $B_\perp$, where the splitting has its minimum value. Within the experimental error ($\Delta E_{10} \simeq 2$ cm$^{-1}$) this definition is equivalent to the more convenient criterion that both resonances are of equal intensity. Resulting values are shown in Fig. 8 as a function of tilt angle. Solid and open symbols denote results measured with and without LED illumination prior to the experiments, respectively.

For half-field coupling ($r = 2$), the gap center is determined correspondingly from the positions of the split resonances *a* and *b*. In this case, the gap center can also be determined as the mean value of the maximum energy of resonance *a* and the minimum energy of resonance *b*, evident in Fig. 6(b), for tilt angles $\theta = 30°$ and $\theta = 39°$. Within an uncertainty $\simeq 2$ cm$^{-1}$, all methods yield the same gap center.

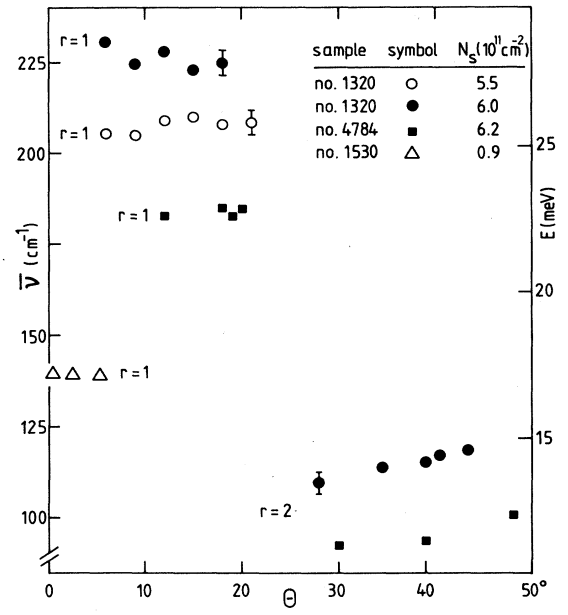


FIG. 8. Energies of gap centers $\bar{E}$ for full-field ($r=1$) and half-field ($r=2$) coupling. Solid and open symbols denote data with and without LED illumination prior to the experiments, respectively.

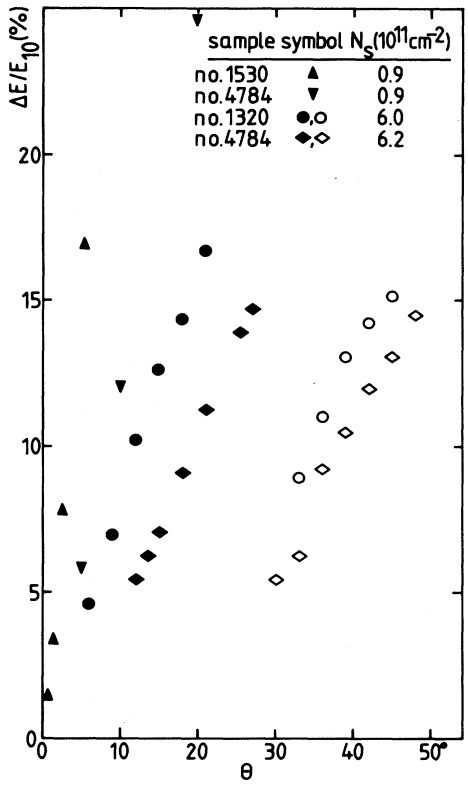


FIG. 9. Normalized splittings at full-field coupling (solid symbols) and half-field coupling (open symbols). Experimental conditions are given in Table I.

In all samples we have studied, the gap centers of half-field coupling shift to higher energies as the tilt angle is increased. This agrees with the theoretical result in Fig. 2(b) and is caused by the diamagnetic shift due to the parallel magnetic field component $B_{\parallel}$. For the gap center of full-field coupling, our simple model in Sec. II predicts a negative shift. However, the experimental results ($r=1$) in Fig. 8 show slightly negative as well as slightly positive shifts. In particular, the sign of the shift seems to depend on the illumination with visible light or electron density $N_s$, as is seen for sample no. 1320 in Fig. 8.

Intersubband energies $E_{10}$ are obtained when the gap centers $\bar{E}$ of full-field coupling are extrapolated to zero tilt angle. The resulting values agree well with those of half-field coupling measured at angles $\theta \simeq 30°$. In Fig. 8 the extrapolated $r=1$ values 231 and 182 $cm^{-1}$ of the illuminated samples no. 1320 and no. 4784 must be compared to the $r=2$ values $2\times 110$ and $2\times 92$ $cm^{-1}$, respectively.

Magnitudes of splittings $\Delta E$ are depicted in Fig. 9 normalized to the measured intersubband energy $E_{10}$. Solid and open symbols stand for full-field and half-field coupling, respectively. According to Eq. (2), the normalized splitting $\Delta E/E_{10}$ for full-field coupling is proportional to the matrix element $z_{10}$ and to the tilt angle $\theta$, provided that the angle is small enough. Within the experimental error, which is approximately as large as the size of the symbols, the latter is observed in Fig. 9. This confirms the applicability of perturbation theory. For different samples, e.g., no. 1530 and no. 4784, we note markedly different slopes of the points in Fig. 9. This indicates largely different matrix elements, since intersubband energies[10] vary by less than a factor of 2.

Well-resolved splittings $\Delta E \gtrsim 1$ meV for half-field coupling can only be detected at tilt angles $\theta \gtrsim 30°$. From the theoretical result shown in Fig. 2(a), we expect an increase of the splitting roughly proportional to the power $\theta^2$. This is consistent with the experimental data in Fig. 9, since linear extrapolation to smaller splittings would lead to zero splittings at angles $\theta \simeq 20°$. Matrix elements of the $z$ coordinate that describe the coupling of electric subbands according to the Hamiltonian of Eq. (1) cannot readily be determined from the observed splittings. As was already pointed out in Sec. II A, virtually all matrix elements $z_{i'i}$ and $(z^2)_{i'i}$ contribute to the splitting at half-field coupling. For the same reason, its quantitative description will provide a very sensitive test for realistic self-consistent surface potentials.

In Table I intersubband energies and dipole matrix elements of three of our samples are compiled and compared with results obtained from literature data.[7,8] The experimental errors are estimated to be $\Delta N_s \simeq 0.1\times 10^{11}$ $cm^{-2}$, $\Delta E_{10} \simeq 0.2$ meV, and $\Delta z_{10} \simeq 0.2$ nm. Sample no. 1530 exhibits an astonishingly large matrix element $z_{10}=9.2$ nm, which may be related to its low intersubband energy $E_{10}=17.2$ meV, as will be discussed in Sec. V. The data for sample no. 1320 demonstrate that the in-

TABLE I. Electron densities $N_s$, intersubband resonance energies $E_{10}$, and dipole matrix elements $z_{10}$. Results obtained from the nonresonant ($\hbar\omega_{c\perp} \lesssim E_{10}/2$) and resonant ($\hbar\omega_{c\perp} \simeq E_{10}$) regime are indicated by $r=\infty$ and $r=1$, respectively. "LED" means "illumination with band-gap radiation prior to the experiment." The intersubband energies required to evaluate the matrix element from Eq. (4), taken from full-field coupling, are in parentheses.

| Sample no. | Remarks | $N_s$ ($10^{11}$ cm$^{-2}$) | $E_{10}$ (meV) | $z_{10}$ (nm) |
|---|---|---|---|---|
| 1530 | $r=1$ | 0.9 | 17.2 | 9.2 |
| 1320 | $r=1$ | 5.5 | 25.4 | 2.4 |
| 1320 | $r=1$ LED | 6.0 | 28.6 | 1.8 |
| 1320 | $r=\infty$ | 5.1 | (25.4) | 3.1 |
| 1320 | $r=\infty$ LED | 6.3 | (28.6) | 2.2 |
| 4784 | $r=1$ | 3.2 | 19.3 | 1.0 |
| 4784 | $r=1$ LED | 6.2 | 22.5 | 1.2 |
| 4784 | $r=1$ gated | 0.9 | 18.8 | 3.8 |
| Schlesinger *et al.*[a] | $r=1$ gated | 1.5 | 24.3 | 3.5 |
| Rikken *et al.*[b] | $r=1$ gated | ~2.0 | 20.3 | 3.1 |

[a] Reference 7.
[b] Reference 8.

tersubband energy increases when the electron density is increased by LED illumination. They also show that matrix elements determined from the nonresonant regime ($r=\infty$) with the aid of Eq. (4) agree well with those obtained from the splitting at full-field coupling ($r=1$) using Eq. (2) for $n=1$. The intersubband energies which are required to evaluate the matrix element from Eq. (4) are taken from full-field coupling and, hence, are put in parentheses. In this analysis, again we only take into account the interaction with subband $i'=1$.

## V. DISCUSSION AND CONCLUSION

It is well known from intersubband resonance experiments, e.g., on Si, that the resonance does not appear at the energy of the suband separation when the light is polarized in the $z$ direction perpendicular to the electron layers.[1,34] Instead, it is shifted to a higher value because each electron "feels" a dynamically screened electric field which is different from the one of the incident radiation, due to the polarization of all the other electrons. This has been described by the sum of two terms, namely the depolarization and exciton-like effect.[15] A dimensionless parameter $\gamma$ has been introduced which relates the observed resonance energy $\tilde{E}_{10}=(1+\gamma)^{1/2}E_{10}$ to the subband separation in the notation of Ref. 15. Since the depolarization term dominates the shift in GaAs/$Ga_{1-x}Al_xAs$ heterojunctions,[35] for brevity we speak here of the total shift as the depolarization shift.

Normally, one needs $z$ polarization to observe the depolarization-shifted intersubband resonance.[36] For the present situation of parallel light polarization and tilted magnetic fields, however, it was recently shown that the experimental resonance positions and splittings ($r=1$) are best described by a model that includes the depolarization effect.[35] This agrees with analytical results[37] obtained in the limit $\gamma \ll 1$. They predict that the gap center ($r=1$), i.e., the intersubband energy, is depolarization shifted by the same amount as the resonance is probed with $z$-polarized light. Intuitively, this may be explained by the fact that the $z$ component of the Lorentz force, which results from the acceleration parallel to the inversion layer, excites the electrons into the $z$ direction, as does the $z$-polarized electric light field.

We have recently measured the depolarization shift in a heterojunction of density $N_s=2.2\times10^{11}$ cm$^{-2}$ and subband separation $E_{10}=19.8$ meV with $z$-polarized light.[12] For this sample, we found a parameter $\gamma=0.09$ much smaller than unity. A direct experimental confirmation, however, that the energies in Table I represent depolarization-shifted values is difficult, since the thick metallization indispensible for experiments with perpendicular light polarization[38] renders difficult experiments with normally incident radiation of parallel polarization on the same sample.

After all, the depolarization shift is a small contribution of $\simeq 1-2$ meV to the observed intersubband energy $\simeq 20$ meV. On the other hand, it can be measured with the relatively high precision $\simeq 0.1$ meV.[12] Thus, its description provides a crucial test for theories of the depolarization and exciton-like shift.

The dependence of intersubband energies $E_{10}$ on electron density $N_s$ tuned by the dose of band-gap radiation is discussed in Ref. 10. Qualitative agreement between experimental data and calculated values[39] is found if depletion charge densities $N_{\rm depl}\simeq 5\times10^{10}$ cm$^{-2}$ are assumed. This agrees rather well with the more recent analysis of Ref. 35, where a density $N_{\rm depl}=6.2\times10^{10}$ cm$^{-2}$ equivalent to a homogeneous acceptor density $N_A=1.8\times10^{14}$ cm$^{-3}$ in the GaAs buffer layer is reported.

According to the theory in Ref. 37, the splitting at full-field coupling ($r=1$) is not affected by the depolarization shift in the limit $\gamma \ll 1$. Nevertheless, its description in terms of a dipole matrix element by the perturbational result of Eq. (2) only is justified as long as the relative shift $\simeq\gamma/2$ of the subband separation is small compared to unity. This must be assumed, since we consider normalized splittings $\Delta E/E_{10}$ in Eq. (2). However, the error of the matrix elements caused by the use of depolarization-shifted values from Table I is estimated to be only 0.1–0.2 nm.

Since matrix elements of self-consistent wave functions have not yet been published, we can only qualitatively discuss their values given in Table I. They vary in a wide range depending on electron density and experimental conditions. The large matrix element of sample no. 1530

indicates a relatively weak interface potential $V(z)$ of comparatively large extent in $z$ direction, presumably due to a low depletion charge density. Also, the high mobility $\mu \simeq 2\times 10^6$ cm$^2$ V$^{-1}$ s$^{-1}$ of this sample, which is extracted from the linewidth of cyclotron resonance in perpendicular magnetic fields,[25] is consistent with this interpretation. In such a situation, nonresonant coupling to higher subbands $i' \geq 2$ may become very effective, and evaluation of an intersubband matrix element according to Eq. (2) should be substantiated by a self-consistent calculation. Generally, it is clear that the values of intersubband matrix elements sensitively probe the interface potential.

Table I also provides important information on the change of the interface potential along with the persistent photoeffect.[40,41] The latter is obvious from data for sample no. 4784. By LED illumination, the electron density $N_s$ increases by almost a factor of 2. Simultaneously, the intersubband energy increases by 3.2 meV, whereas the matrix element slightly increases or, at best, remains constant within the experimental error $\Delta z_{10} \simeq 0.2$ nm. This cannot be understood even qualitatively within the triangular-well approximation, which predicts[17] a subband spacing proportional to $(z_{10})^{-2}$. The same conclusion must be drawn if depletion by a gate voltage is considered. Indeed, as is qualitatively expected, the intersubband energy decreases and the matrix element increases when the density is decreased by a gate voltage. However, the decrease of the intersubband energy again is not proportional to $(z_{10})^{-2}$.

It was found in Ref. 39 that the triangular-well approximation does not provide a good description for the energy $E_1$ of the excited subband but does for the energy of the ground subband $E_0$. This makes its failure to grasp matrix elements involving wave functions of higher subbands understandable.

To summarize, we have measured the far-infrared transmittance of $n$-type GaAs/$Ga_{1-x}Al_xAs$ heterojunctions in tilted magnetic fields. This arrangement is very effective for the study of the subband structure of the underlying quasi-two-dimensional electron layers, particularly in three respects. First, from the positions of split cyclotron resonances observed with light polarized parallel to the layers, we can determine intersubband energies, i.e., depolarization-shifted subband separations. Second, we were able[12] to measure many-body effects, namely the depolarization and exciton-like shift, with perpendicular light polarization in tilted magnetic fields. To achieve this, we compared the resonance positions of combined intersubband-cyclotron resonances $E_{10} \pm \hbar\omega_{c\perp}$ with the position of the $B = 0$ intersubband resonance.[12,15] Third, we can measure dipole or intersubband matrix elements $z_{10}$ from the magnitude of the splitting at full-field coupling ($\hbar\omega_{c\perp} \simeq E_{10}$) as well as from the mass enhancement in the nonresonant regime ($\hbar\omega_{c\perp} \ll E_{10}$). The latter method is much more convenient, since laboratory magnetic field strengths $B \lesssim 10$ T suffice. We also would like to add that this method is quite universal and has, in fact, been successfully applied to other quasi-two-dimensional systems, such as coupled GaAs quantum wells.[42]

## ACKNOWLEDGMENTS

We thank K. Ensslin, D. Heitmann, J. P. Kotthaus, J. C. Maan, and H. Sigg for valuable discussions, and acknowledge financial support of the Deutsche Forschungsgemeinschaft. We also would like to thank the Hochfeldlabor of the Max-Planck-Institut für Festkörperforschung in Grenoble, France, where part of the measurements were carried out, for their hospitality.

*Present address: Max-Planck-Institut für Festkörperforschung, Heisenbergstrasse 1, Postfach 80 06 65, D-7000 Stuttgart 80, West Germany.

†Present address: Walter-Schottky-Institut der Technischen Universität München, D-8046 Garching bei München, West Germany.

[1]T. Ando, A. B. Fowler, and F. Stern, Rev. Mod. Phys. **54**, 437 (1982).

[2]F. Koch, in *Physics in High Magnetic Fields,* Vol. 24 of *Springer Series in Solid-State Sciences,* edited by S. Chikazumi and N. Miura (Springer, Berlin, 1981), pp. 262–273.

[3]J. H. Crasemann and U. Merkt, Solid State Commun. **47**, 917 (1983).

[4]J. C. Maan, in *Infrared and Millimeter Waves,* edited by K. J. Button (Academic, New York, 1983), Vol. 8, Chap. 9, pp. 387–426.

[5]M. A. Brummell, M. A. Hopkins, R. J. Nicholas, J. C. Portal, K. Y. Cheng, and A. Y. Cho, J. Phys. C **19**, 107 (1986).

[6]F. F. Fang and P. J. Stiles, Phys. Rev. **174**, 823 (1968).

[7]Z. Schlesinger, J. C. M. Hwang, and S. J. Allen, Jr., Phys. Rev. Lett. **50**, 2098 (1983). Equation (7) should read $E_{\pm} = E_{10} \pm \frac{1}{2}\hbar\omega_c \sin\theta$.

[8]G. L. J. A. Rikken, H. Sigg, C. J. G. M. Langerak, H. W. Myron, J. A. A. J. Perenboom, and G. Weimann, Phys. Rev. B **34**, 5590 (1986).

[9]A. D. Wieck, J. C. Maan, U. Merkt, J. P. Kotthaus, and K. Ploog, in *Proceedings of the 17th International Conference on the Physics of Semiconductors,* edited by O. Engström (World Scientific, Singapore, 1987), Vol. 1, p. 601.

[10]A. D. Wieck, J. C. Maan, U. Merkt, J. P. Kotthaus, K. Ploog, and G. Weimann, Phys. Rev. B **35**, 4145 (1987).

[11]W. Beinvogl and J. F. Koch, Phys. Rev. Lett. **40**, 1736 (1978).

[12]A. D. Wieck, K. Bollweg, U. Merkt, G. Weimann, and W. Schlapp, Phys. Rev. B **38**, 10 158 (1988).

[13]J. C. Maan, in *Two-Dimensional Systems, Heterostructures, and Superlattices,* Vol. 53 of *Springer Series in Solid-State Sciences,* edited by G. Bauer, F. Kuchar, and H. Heinrich (Springer, Berlin, 1984), pp. 183–191.

[14]R. Merlin, Solid State Commun. **64**, 99 (1987).

[15]T. Ando, Phys. Rev. B **19**, 2106 (1979).

[16]This choice differs by a phase factor from the one of Ref. 15.

[17]S. Oelting, A. D. Wieck, E. Batke, and U. Merkt, Surf. Sci. **196**, 273 (1988).

[18]S. J. Allen, Jr., D. C. Tsui, and B. Vinter, Solid State Commun. **20**, 425 (1976).

[19]W. P. Chen, Y. J. Chen, and E. Burstein, Surf. Sci. **58**, 263

(1976).
[20]T. Ando, Solid State Commun. **21**, 801 (1977).
[21]R. G. Gordon, J. Chem. Phys. **51**, 14 (1969). Integrals over Airy functions are treated in Appendix B.
[22]R. Dingle, H. L. Störmer, A. C. Gossard, and W. Wiegmann, Appl. Phys. Lett. **33**, 665 (1978).
[23]G. Weimann and W. Schlapp, Appl. Phys. Lett. **46**, 411 (1985).
[24]K. Ploog, J. Cryst. Growth **79**, 887 (1986).
[25]F. Thiele, W. Hansen, M. Horst, J. P. Kotthaus, J. C. Maan, U. Merkt, K. Ploog, G. Weimann, and A. D. Wieck, in *High Magnetic Fields in Semiconductor Physics,* Vol. 71 of *Springer Series in Solid-State Sciences,* edited by G. Landwehr (Springer, Heidelberg, 1987), pp. 252–255.
[26]E. Batke and D. Heitmann, Infrared Phys. **24**, 189 (1984).
[27]F. Thiele, U. Merkt, J. P. Kotthaus, G. Lommer, F. Malcher, U. Rössler, and G. Weimann, Solid State Commun. **62**, 841 (1987).
[28]M. A. Hopkins, R. J. Nicholas, M. A. Brummell, J. J. Harris, and C. T. Foxon, Phys. Rev. B **36**, 4789 (1987).
[29]M. Horst, U. Merkt, W. Zawadzki, J. C. Maan, and K. Ploog, Solid State Commun. **53**, 403 (1985).
[30]H. Sigg, P. Wyder, and J. A. A. J. Perenboom, Phys. Rev. B **31**, 5253 (1985).
[31]R. Lassnig and E. Gornik, Solid State Commun. **47**, 959 (1983).
[32]K. Ensslin, D. Heitmann, H. Sigg, and K. Ploog, Phys. Rev. B **36**, 8177 (1987).
[33]E. Batke, H. L. Störmer, A. C. Gossard, and J. H. English, Phys. Rev. B **37**, 3093 (1988).
[34]D. Heitmann and U. Mackens, Phys. Rev. B **33**, 8269 (1986).
[35]K. Ensslin, D. Heitmann, and K. Ploog, in *High Magnetic Fields in Semiconductor Physics II, Springer Series in Solid State Sciences,* edited by G. Landwehr (Springer, Berlin, in press).
[36]K. Wiesinger, H. Reisinger, and F. Koch, Surf. Sci. **113**, 102 (1982).
[37]K. Załużny, Solid State Commun. **55**, 747 (1985); **56**, 235 (1985).
[38]B. D. McCombe, R. T. Holm, and D. E. Schafer, Solid State Commun. **32**, 603 (1979).
[39]F. Stern and S. Das Sarma, Phys. Rev. B **30**, 840 (1984).
[40]E. F. Schubert, A. Fischer, and K. Ploog, Phys. Rev. B **31**, 7937 (1985).
[41]L. X. He, K. P. Martin, and R. J. Higgins, Phys. Rev. B **36**, 6508 (1987).
[42]A. Lorke, A. D. Wieck, U. Merkt, G. Weimann, and W. Schlapp, in Proceedings of the Fourth International Conference on Superlattices, Microstructures, and Microdevices (Trieste, 1988) [Superlatt. Microstruct. (to be published)].